A Microgrid Energy Management System Based on the Rolling Horizon Strategy

Rodrigo Palma-Behnke, *Senior Member, IEEE*, Carlos Benavides, Fernando Lanas, Bernardo Severino, Lorenzo Reyes, Jacqueline Llanos, *Student Member, IEEE*, and Doris Sáez, *Senior Member, IEEE*

***Abstract*—A novel energy management system (EMS) based on a rolling horizon (RH) strategy for a renewable-based microgrid is proposed. For each decision step, a mixed integer optimization problem based on forecasting models is solved. The EMS provides online set points for each generation unit and signals for consumers based on a demand-side management (DSM) mechanism. The proposed EMS is implemented for a microgrid composed of photovoltaic panels, two wind turbines, a diesel generator and an energy storage system. A coherent forecast information scheme and an economic comparison framework between the RH and the standard unit commitment (UC) are proposed. Solar and wind energy forecasting are based on phenomenological models with updated data. A neural network for two-day-ahead electric consumption forecasting is also designed. The system is tested using real data sets from an existent microgrid in Chile (ESUSCON). The results based on different operation conditions show the economic sense of the proposal. A full practical implementation of the system for ESUSCON is envisioned.**

***Index Terms*—Demand-side management, energy management system, microgrid, photovoltaic, rolling horizon, wind turbine.**

I. Introduction

WITH A LOW population density and many natural resources, Chile's electricity supply shortage is a paradox. The Atacama Desert, Andes Mountains, long coastline, and strong agriculture provide the country with abundant distributed renewable energy resources that could, according to recent estimations, largely surpass the fast-growing electricity demand. In addition, because of the geographic conditions of extreme points in Chile, there are still several small settlements deep into the mountains that are isolated from the interconnected power system. In this context, renewable-based technologies offer a solution for gathering the distributed energy resources [1].

A renewable-based microgrid can be understood as a particular case of a more general concept called a 'smart grid', which is an interdisciplinary term for a set of technological solutions for electric power system management. Smart grids are understood to be the key enabling technology for renewable energy development, electric vehicle adoption and energy efficiency improvements [2]. Smart grids represent a vision for digital optimization of electric power distribution and transmission grids as applied to current operations, enhancing the grid security and opening up new ways of tapping alternative energy sources. By using the Internet protocol on home devices, the smart grid would be able to shuttle information back and forth between the distributed electric utilities and customers.

In the specialized literature, there are works related to energy management system (EMS) for microgrids. In [3], an online power energy management for a hybrid fuel cell/battery distributed generation system is presented. The online architecture consists of three layers: the first one captures the possible operations modes, the second is based on a fuzzy controller for power splitting between batteries and fuel cells, and the last one regulates each subsystem.

In [4], an EMS for controlling a virtual power plant (VPP) is presented. In this case, the objective is to manage the power flows to minimize the electricity generation costs and to avoid the loss of energy produced by renewable energy sources. The VPP is composed of combined heat and power plants, wind parks and a photovoltaic plant. The surplus energy generated by renewable units is used for the operation of both a desalination plant and an electrolyzer that provide hydrogen for industrial processes. Lu & Francois [5] describe an energy management system based on day-ahead power scheduling for a microgrid (photovoltaic panels, gas turbine) that considers the power prediction and load forecasting. The EMS provides the real-time power set points for microgrid units and coordinates the droop controllers for the primary frequency control.

In Teleke *et al.* [6], a rule-based control strategy is designed for a battery energy storage system with photovoltaic arrays and a wind farm. The renewable sources can be dispatched hourly, based on forecasting of the solar and wind conditions. The rule-based controller determines the current reference for the converter that will charge/discharge the battery bank by using the state of charge (SOC) and the battery voltage. This system can deal with variability in the wind and solar generation. Wang *et al.* [7] designed a power management system for a stand-alone grid that is composed of a wind turbine, photovoltaic arrays and a fuel cell. The proposed management system is tested for different scenarios by using a practical load demand profile and real weather data. The strategy coordinates the power flows among the different energy sources.

Gupta *et al.* [8] developed steady-state models for a hybrid energy system for determining its optimal operation. The hybrid system is composed of microhydro, biogas, biomass, photovoltaic panels, a battery bank and a fossil fuel generator. An

Manuscript received July 04, 2011; revised November 18, 2011, June 15, 2012, and August 31, 2012; accepted October 14, 2012. Date of publication January 22, 2013; date of current version May 18, 2013. This work was supported in part by the mining company Doña Inés de Collahuasi, the Millennium Institute "Complex Engineering Systems" (ICM: P-05-004-F, CONICYT: FBO16), and FONDECYT project 1110047. Paper no. TSG-00233-2011.

The authors are with the Energy Center, Faculty of Mathematical and Physical Sciences, School of Engineering, University of Chile (CMM, ISCI, DIE), Av. Tupper 2007, 8370451, Santiago Chile (e-mail: rodpalma@cec.uchile.cl; dsaez@ing.uchile.cl).

Color versions of one or more of the figures in this paper are available online at http://ieeexplore.ieee.org.

Digital Object Identifier 10.1109/TSG.2012.2231440

economic dispatch strategy with mixed integer linear programming is implemented. Westermann and John [9] describe a combination of wide-area measurement and ripple control for DSM. The proposed control systems moderate the impact of increased renewable sources on adjacent transmission grids. Hamidi and Robinson [10] propose a responsive demand for a system with significant intermittent generation, e.g., a microgrid with renewable sources. In this system, the demand can shift to reduce the peak and also be reduced to mitigate the power fluctuations; however, this action requires evaluating the value of the lost load for consumers.

Lagorse and Somoes [11] propose a distributed EMS to control the energy flow in the hybrid energy system (HES). This distributed controller is based on multiagent-system (MAS) technology. The hybrid system is composed of photovoltaic cells, batteries, fuel cells, supercapacitor and load. The battery unit is guided by fuzzy-logic rules. Logenthiran and Srinivasan [12] describe a three-step efficient method for the optimal generation scheduling of a microgrid in island operation. This microgrid is composed of a photovoltaic system, a wind park, thermal units and a battery bank. The first step is to set up an initial feasible solution for thermal unit commitment, considering the use of renewable energy to meet the load. From these solutions, the start-up and shut-down of thermal units is determined, again solving a thermal unit commitment problem. The final step is to optimize a nonlinear renewable-thermal dispatch, considering the nonlinear constraints associated with the modeling of renewable energy sources and assuming the start-ups and shut-downs of thermal units are known. The nonlinear optimization problem is solved using genetic algorithms.

Tsikalakis and Hatziargyriou [13] describe a centralized control system for a microgrid. The controller is used to optimize the operation of the microgrid during interconnected operation, i.e., the production of local generators and energy exchanges with the distribution network are maximized. Two market policies are assumed to offer options for the demand for controllable loads, and this demand-side bidding is incorporated into the centralized control system.

With regard to EMS with rolling horizon used in the field of smart grids, Dagdougui *et al.* [14] describe a real time operational management system for a hybrid renewable system, composed of an electrolyzer, a hydroelectric plant, pumping stations, a wind turbine and a fuel cell. The goal is to satisfy the variable electric, hydrogen, and water demands hourly. Morais *et al.* [15] present an optimal dispatch of micro-grid renewable energy park. The microgrid is composed of photovoltaic panels, wind turbines, a fuel cell, a load, and a storage battery. The dispatch is based on the minimization of the generation costs and the optimization of the storage charging and discharging cycles. Korpas and Holen [16] present an EMS system for a hybrid plant with wind power and hydrogen storage. The system maximizes the expected profit from power trading in a day-ahead market based on forecast information for generation, load, and electricity price. In the studies cited, basic forecast data information for the electric demand and renewable energy availability is used. Additionally, the economic benefits of the control strategies are not explicitly evaluated.

The aforementioned characteristics and research proposals are applicable to a smart microgrid concept. An isolated grid with these new features is able to offer new development opportunities and perspectives for the local community. The resulting solution is also able to be interconnected to a power grid as a microgrid solution, allowing the integration of the local energy resources. In this work, based on a specific real location in the north of Chile, a novel EMS based on a rolling horizon strategy for a renewable-based microgrid is proposed. For each decision step, a mixed integer optimization problem based on forecasting models is solved. The EMS considers a two-day-ahead forecast of renewable sources and a two-day-ahead prediction for electric consumption based on a neural network model. In addition, EMS integrates a DSM scheme that provides signals for consumers [1]. Nevertheless, in this proposal [1], the uncertainties are not considered explicitly.

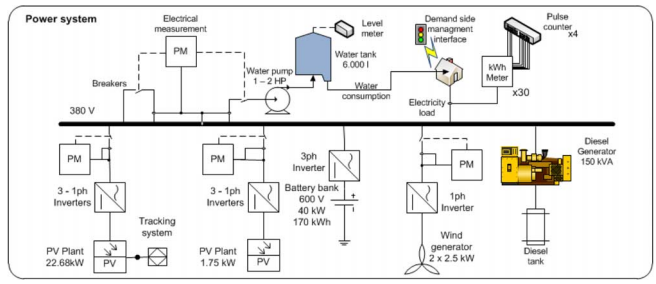

Fig. 1. Renewable-based microgrid: Power schematic.

The EMS includes an objective function and the nonlinear constraints associated with the modeling of both units. These constraints are represented by piecewise linear models, binary variables and so forth. Therefore, the optimization problem is solved using mixed integer linear programming, ensuring the near-optimality. This advantage is not present in the previous works described that used Lagrange relaxation, genetic algorithms and others.

The rest of the paper is organized as follows: In Section II, a description of the renewable-based microgrid and its current power system is given. In Section III, a description of communication infrastructure of the renewable-based microgrid is presented. Section IV details the proposed energy management system, including the modeling of each unit and the DSM. In Section V, simulation results are presented and analyzed under different scenarios. Section VI concludes the paper.

II. Description of the Renewable-Based Microgrid

The microgrid had been conceived for a small, isolated village in the Atacama Desert, Chile, called Huatacondo $(20°55'36.37''S69°3'8.71''W)$. Its electric network was isolated from the interconnected system and was supplied only 10 hours a day by a diesel generator. This microgrid takes advantage of the distributed renewable resources in the area, providing 24-hour electricity service. Because the village experienced problems with the water supply system, a management solution was also included in the microgrid. Additionally, a demand-side option to compensate the generation fluctuations due to the renewable sources was considered. The system is composed of two photovoltaic systems, a wind turbine, the existing diesel generator unit of the village (typical in isolated locations), an energy storage system (ESS) composed of a lead-acid battery bank (LABB) connected to the grid through a bidirectional inverter, a water pump and a DSM (loads). Fig. 1 summarizes the power schematic of this microgrid.

The following are the main goals of the EMS:

- Minimize the use of diesel

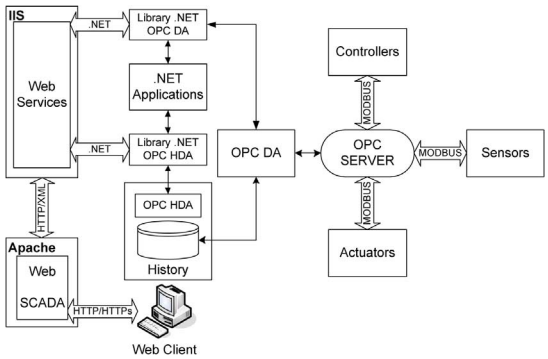

Fig. 2. Renewable-based microgrid: SCADA hardware.

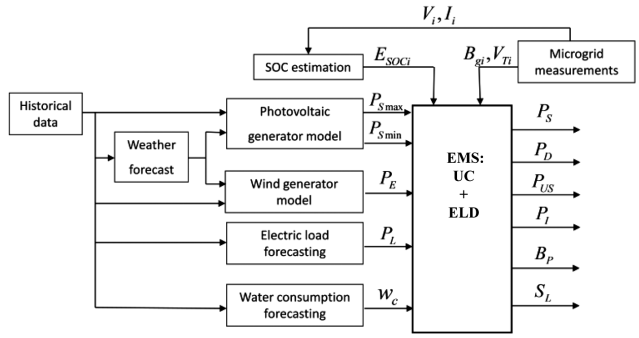

Fig. 3. Blocks diagram of the proposed energy management system.

- Deliver active generation set points for the diesel generator, the ESS inverter, and the PV plant
- Turn on and off the water pump in order to keep the elevated water tank level within predefined limits
- Send signals to consumers promoting behavior changes

In field implementation, the diesel generator and the ESS inverter have two configurable droop curves to follow the set points. Q-V and P-f droop curves are normally configured for typical operation states that change when receiving adequate signals from the EMS.

When the EMS turns on the diesel generator, it is convenient to start the LABB charge. In that case, the diesel generator is configured to work in isochronous mode (with infinite slope in both curves, takes all the variations between generation and load, following the rated values $380[V_{l-l}]@50$ [Hz]), and the ESS inverter curves are configured to follow the charging profile of the batteries.

When the diesel generator is turned off, the droop curves of the ESS inverter change to those for a master operation mode, with a very low droop characteristic.

III. Communication Infrastructure

In regard to the communications infrastructure of the proposed renewable-based microgrid, to acquire the field data for optimizing the operation of the system, a SCADA and several measurement devices were installed in the Huatacondo Village (see Fig. 2).

The main server (OPC SERVER) runs a Matrikon OPC Data Access Service (OPC DA) using an Ethernet MODBUS TCP protocol and a Matrikon Historical Data Access Service (OPC HDA) to save historical data [17].

All field devices such as controllers, sensors, and actuators (collecting electrical measurements and status information) communicate through the MODBUS RTU protocol, by using Ethernet/Serial converters for the needed translation.

For the data transfer, NET applications were written using existing GPL libraries that also provide communications with Web Services allowing private web clients to retrieve the real-time and historical data via the Internet.

To collect the information the OPC DA must be configured with several tags. Therefore, timestamps can also be retrieved as a basis for the forecasting algorithms. The server is configured to read variables every second and to store them in the database every 10 seconds.

In summary, for the communication between devices, the microgrid uses a SCADA with the following capabilities:

- Electrical variable measurements for all generation units,
- Some electrical measurements in the grid and control capabilities (connection/disconnection of low voltage network feeders).
- Energy consumption measurement of the electrical loads in the network.
- Power control of the ESS inverter and diesel generator.
- Grid connection control for all generation units and the water pump consumption.
- Sun tracking control for the principal PV plant.
- Wireless communication with the interfaces of the DSM system.

IV. Proposed Energy Management System

A. Problem Statement

The EMS minimizes the operational costs while supplying the water and load demands, considering a two-day-ahead forecasting of the weather conditions, water consumption and electrical load. Fig. 3 shows the proposed EMS that provides the power references for the diesel (P_D) generator, the ESS inverter power (P_I), the binary signals for the water supply system (B_P), the desired solar power (P_S) and the signals for loads (S_L). The EMS inputs are the predicted maximum and minimum attainable solar power (P_{Smax}, P_{Smin}), wind power (P_E), expected load (P_L), water consumption (w_c), initial conditions for the battery charge (E_{SOC_i}), battery bank voltage (V_i) and current (I_i), water tank level (V_{Ti}) and diesel on/off state (B_{gi}).

For the design of the EMS, the objective function, the power balance and the dynamic model of the generation units with their corresponding mixed integer programming (MIP) formulations are presented. The EMS is solved at the supervisory level using a unit commitment (UC) with a rolling horizon strategy (UC-RH).

The rolling horizon is considered for reducing the effect of the uncertainties of the input variable forecasting. Thus, the UC-RH control strategy at the supervisory level includes the following steps:

1) Get the initial condition for $t = t_{initial}$.
2) The EMS optimizes the system operation for the periods from $t_{initial}$ to $t_{initial} + T$ (T: prediction horizon) using forecasting for the input variables and the initial conditions of the units. In this case, the prediction horizon is two days, 192 steps with a sampling time of 15 minutes.
3) Obtain the optimal set points of units for T.
4) Apply the set points obtained in step 2 for a shorter period than T, in this case, t to $t + \Delta - 1$.
5) Adjust the set points for dispatchable units based on current (measured) load and non-controllable renewable injections

in the system. For the ESS the opportunity cost of the stored energy is considered. An economic load dispatch (ELD) is used for this purpose. The update period of the ELD can be flexible, selected between 1 and 5 minutes.

6) Update $t = t_{initial} + \Delta$.
7) Return to step 1.

B. Objective Function

The objective function of EMS is to minimize the operational costs of the microgrid in a time scope (T). The objective function is formulated as

$$J = \delta_t \sum_{t=1}^{T} C(t) + \sum_{t=1}^{T} C_s(t) + C_{US}\delta_t \sum_{t=1}^{T} P_{US}(t) + C_{Tf} \sum_{t=1}^{T} V_{Tf}(t) + C_H(T) \quad (1)$$

where δ_t is the duration of time period t, $C(t)$ is the cost function of the diesel generator, $C_s(t)$ is the start-up cost function of diesel generator, $P_{US}(t)$ is the unserved power in the system, $C_{US}(t)$ is the price for unserved energy, $V_{Tf}(t)$ is the unserved water, $C_{Tf}(t)$ is the cost of unserved water and $C_H(T)$ is the cost of using the LABB. The first term of the objective function (1) represents the diesel costs, the second term the start-up diesel cost and the next two terms penalize the unsupplied electric energy and the unserved water supply, respectively. The last term represents the cost penalty of using the LABB and affecting its lifetime in different ways.

C. Power Balance for the Microgrid

The power balance in the microgrid must be satisfied:

$$P_D(t) + P_I(t) + P_{US}(t) = P_L(t) + B_P(t)\bar{P}_P - P_{Lost}(t) - P_S(t) - P_E(t) \quad (2)$$

where $P_L(t)$ is the electrical load, $\overline{P}_P$ is the rated pump power, $P_{Lost}(t)$ is the unused power from the energy sources (storage was not possible). Additional constraints for the problem are $P_{US}(t) \geq 0$ and $P_{Lost}(t) \leq 0$.

D. Modeling of Renewable Energy Units

1) Photovoltaic Panels: In the model proposed, the solar power is controlled by the east-to-west inclination angle of the panels (α). The maximum power $P_{Smax}(t)$ is obtained by the optimal orientation of the PV panels. Sometimes, it is not feasible to use the maximum solar power because, for example, the ESS is completely charged. To prevent this problem, the minimum power $P_{Smin}(t)$ is obtained when the photovoltaic panels are oriented to the minimum irradiance subject to the panel structure physical constraints. Therefore, the solar power $P_S(t, \alpha)$ will be a value between these bounds, which are as follows:

$$P_S(t, \alpha) = \eta_S A_S R_S(t, \alpha) \quad (3)$$

$$P_{Smin}(t) \leq P_S(t, \alpha) \leq P_{Smax}(t) \quad (4)$$

where η_S is the solar panel efficiency, A_S is the total plant surface and $R_S(t, \alpha)$ is the irradiance perpendicular to the panel's plane.

2) Wind Generator: Generally, wind power may be obtained using the wind turbine profile given by the manufacturer. In this case, a piecewise linear approximation of the profile was incorporated into the wind generator model.

When this is not possible, the wind power maybe calculated based on the wind speed and the wind turbine power coefficient obtained from the basic model expression [18].

E. Forecasting Models

1) Solar Irradiance: For horizontal solar irradiance forecasting based on the persistency methodology, the clear-sky index (k^*) is used [19], which is an approximate measurement for cloudy conditions right above the sensor location:

$$k^*(t) = \frac{\tilde{R}_S(t)}{R_{CS}(t)}, \quad k^*(t) \rightarrow \begin{cases} 1 & clearly\ day \\ 0 & nubosty\ day \end{cases} \quad (5)$$

$\tilde{R}_S(t)$ is the measured irradiance and $R_{CS}(t)$ is the irradiance calculated with a phenomenological clear-sky model. With this model, measured errors increase during the sunset and at dawn. Hence, (5) is used in cases in which the solar altitude is greater than 20°, as recommended in [19].

Then, for the predicted irradiance $\hat{R}_S$, k^* is assumed to be an average of the past indices, as shown in (6).

$$\hat{R}_s(t+1) = R_{CS}(t+1) \times \frac{1}{n} \sum_{i=0}^{n-1} k^*(t-i) \quad (6)$$

where n is the number of model autoregressors. The proposed approach currently has detractors because of the RMSE values obtained in field measurements [19]. Nevertheless, given the special conditions in the north eastern part of the country (Atacama Desert), the proposed model is suitable for a two-day-ahead prediction.

2) Wind Speed: For forecasting the wind speed, this work considers a global forecast system (GFS) for the bounded conditions of a weather research and forecast (WRF) model [20], [21].

The GFS model is used for determining the border conditions of the wind speed that the WRF model used as an initial condition. Finally, the results of the WRF model are adjusted using statistical methods for a 12- or a 48-hour-ahead prediction.

3) Electrical and Water Consumption: For load forecasting, neural networks have been widely used. Recently, wavelets have been used for characterizing the load, and then, they are used as inputs for the neural network models [22]. In addition, evolutionary algorithms have been used for determining the inputs for a load model based on fuzzy logic [23]. In this work, the electrical consumption is predicted based on neural network modeling using empirical data. The multilayer architecture is considered with one hidden layer. Backpropagation for determining the weights and a structural optimization process for determining the relevant inputs are used [24]. The same procedure for the water consumption can be used.

F. Modeling of Conventional Generation Units

1) Diesel Generator: The fuel consumption of a diesel generator $q(t)$ can be represented as a non convex function. For the MIP formulation, a non convex function can be approximated by n_v piecewise linear segments. Fig. 4 shows an example for

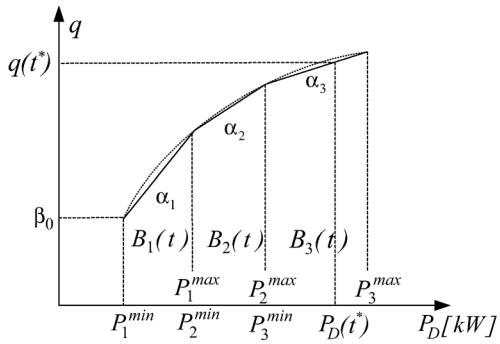

Fig. 4. Nonconvex cost function of the diesel generator, $n_v = 3$.

$n_v = 3$. Each piecewise linear segment v introduces the binary variables $B_v(t)$ and continuous variable $P_v(t)$, analytically:

$$q(t) = \sum_{v=1}^{n_v} (\alpha_v P_v(t) + \beta_v B_v(t)) \tag{7}$$

where α_v is the slope and β_v is the Y-intercept of segment v.

The following constraint is added for imposing that only one variable $B_v(t)$ takes the value 1 in period t:

$$\sum_{v=1}^{n_v} B_v(t) \leq 1 \tag{8}$$

Then, when $\sum_{v=1}^{n_v} B_v(t) = 1$ means the diesel unit is turned-on, otherwise the unit is turned-off.

The generated diesel power $P_D(t)$ is given by:

$$P_D(t) = \sum_{v=1}^{n_v} P_v(t) \tag{9}$$

$$P_v^{min} B_v(t) \leq P_v(t) \leq P_v^{max} B_v(t), \quad v = 1, \ldots, n_v \tag{10}$$

As shown in Fig. 4, if the unit is turned-on the dispatched power $P_D(t)$ at instant t^* takes a value between P_3^{min} and P_3^{max}, and in the (8), the corresponding binary variables are:

$$B_1(t^*) = 0 \; B_2(t^*) = 0 \text{ and } B_3(t^*) = 1 \tag{12}$$

Contrarily, when the diesel unit is turned-off the corresponding binary variables are:

$$B_1(t) = 0 \; B_2(t) = 0 \text{ and } B_3(t) = 0 \tag{13}$$

Then, the cost function is represented by $C(t) = C_C q(t)$, where C_C represents the price of diesel.

The positive variable $C_S(t)$ represents the startup cost of the diesel generator:

$$C_s(t) \geq C_D \left(\sum_{v=1}^{n_v} B_v(t) - B_{g0} \right) \text{t} = 1 \tag{14}$$

$$C_s(t) \geq C_D \left(\sum_{v=1}^{n_v} B_v(t) - \sum_{v=1}^{n_v} B_v(t-1) \right) \text{t} > 1 \tag{15}$$

$$C_s(t) \geq 0 \tag{16}$$

where C_D represents a fixed start-up cost and B_{g0} is the initial condition ($B_{g0} = 1$ if the unit was previously turned-on and $B_{g0} = 0$ if the unit was previously turned-off). This initial condition is obtained from the SCADA.

For example, in (15) if $\sum_{v=1}^{n_v} B_v(t-1) = 0$ and $\sum_{v=1}^{n_v}(t) = 1$, the diesel generator starts up in t, and therefore:

$$C_s(t) \geq C_D(1-0) \Rightarrow C_s(t) \geq C_D \tag{17}$$

Because the startup costs are represented by inequality constraints (14), (15), (16), their values are obtained from the EMS operation that provides the values of the $B_v(t)$ variables, which represent the on-off state of the diesel generator.

The volume of the diesel tank variable $V_D(t)$ is given by:

$$V_D(t) = V_D(t-1) - \left(\sum_{v=1}^{n_v} \alpha_v P_v(t) + \beta_v B_v(t) \right) \tag{18}$$

$$V_{Dmin} \leq V_D(t) \leq V_{Dmax} \tag{19}$$

Additionally, a minimum volume for the diesel tank at the end of the prediction horizon T is included as:

$$V_D(T) \geq V_D^T \tag{20}$$

2) Energy Storage System: A simplified dynamic model of the ESS:

$$E(t) = E(t-1) - \delta_t P_B(t) \tag{21}$$

where $P_B(t)$ is the DC power of the LABB, assuming a positive value if it injects power to the microgrid and a negative value for the charging mode.

The inverter model is:

$$P_I(t) = \begin{cases} \eta_{Id} P_B(t) - P_{I0} & P_B(t) \geq 0 \\ \frac{P_B(t)}{\eta_{Ic}} - P_{I0} & P_B(t) < 0 \end{cases} \tag{22}$$

where P_{I0} is the internal consumption of the inverter. The constants η_{Id} and η_{Ic} are used to represent the losses of the inverter. The corresponding MIP formulation for the inverter model described in (21) is:

$$P_I(t) = \eta_{Id} P_B^+(t) + \frac{P_B^-(t)}{\eta_{Ic}} - P_{IO} \tag{23}$$

$$0 \leq P_B^+(t) \leq P_{\max}^B B_B^+(t) \tag{24}$$

$$M B_B^-(t) \leq P_B^-(t) < 0 \tag{25}$$

The power $P_B^+(t)$ is used when the LABB is discharging, and $P_B^-(t)$ is used for the charging model. $P_{max}^B(t)$ represents the maximum charging power and M is a large negative parameter representing the maximum load power. $B_B^+(t)$ and $B_B^-(t)$ are binary variables associated with each operation mode. Only one operation mode is allowed for a specific time period:

$$B_B^-(t) + B_B^+(t) \leq 1 \tag{26}$$

The MIP formulation of the LABB energy model described in (20) is represented by:

$$E(t) = E(t-1) - \delta_t \eta_B^+ P_B^+(t) - \delta_t \eta_B^- P_B^-(t) \tag{27}$$

$$E_{soc}^{min} E_{max} \leq E(t) \leq E_{soc}^{max} E_{max}, E(T) \geq E_f \tag{28}$$

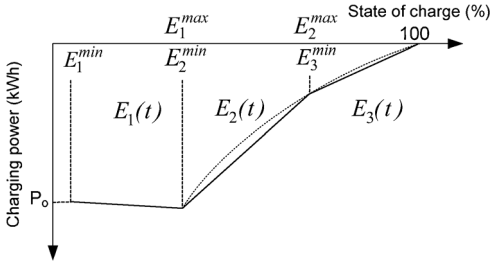

Fig. 5. Minimum admissible power in the LABB vs. the battery bank SOC.

The constants η_B^+ and η_B^- are used to represent the charge and discharge energy efficiency of the LABB. E_{SOC}^{min} is a value between 0 and 1, and it should be chosen depending on the desired depth of discharge of the LABB system. E_{max} is the maximum storage value of the energy bank. E_f is a reference energy value of the LABB.

The constraints for the allowed battery power are:

$$P_{Bmin}\left(E(t-1)\right) \leq P_B(t) \leq P_{Bmax}\left(E(t-1)\right) \tag{29}$$

The minimum admissible power of the LABB (negative value in the model) is related to the maximum charge current that depends on the end of the charge voltage trigger [25]. This charging constraint is shown in Fig. 5. The maximum LABB power P_{Bmax} (positive value in the model) is determined by the current limit of the inverter.

For the MIP formulation of (29), a non convex function to represent the minimum admissible power of the LABB $P_{min}^B(t)$ can be approximated by n_s piecewise linear segments as (see Fig. 5):

$$P_{\min}^B(t) = P_o + \sum_{s=1}^{n_s} \alpha_s^B E_s(t-1) \tag{30}$$

Each piecewise linear segment s introduces the binary variables $B_s(t)$ and the continuous variable $E_s(t)$. α_s^B is the slope of segment s ($s \leq n_s - 1$).

$$\left(E_s^{\max} - E_s^{\min}\right) B_{s+1}(t) \leq E_s(t) \leq \left(E_s^{\max} - E_s^{\min}\right) B_s(t) \tag{31}$$

$$0 \leq E_{n_s}(t) \leq \left(E_{n_s}^{\max} - E_{n_s}^{\min}\right) B_{n_s}(t) \tag{32}$$

where $E_{soc}^{\max} = E_{n_s}^{\max}$, $E_{soc}^{\min} = E_1^{\min}$ and E_s^{min} and E_s^{max} are the upper and lower bounds of segment s.

Thus, the maximum charging power is expressed by:

$$P_B^-(t) \geq P_{\min}^B(t) \tag{33}$$

The energy balance is represented by:

$$E(t) = E_{soc}^{min} + \sum_{s=1}^{n_s} E_s(t) \tag{34}$$

The cost penalty of the LABB is given by the decline in the state of health (*SoH*) of the ESS at the end of the evaluation period.

$$C_H(T) = \left[SoH(T) - SoH(1)\right] \cdot C_I \tag{35}$$

C_I is a factor associated with the investment cost of the LABB. The *SoH* is directly related to the ESS lifetime. The lifetime of the internal components of the battery depends on chemical effects such as corrosion; sulfating or water losses. Therefore *SoH* is mainly determined by both its temperature and its working zone [26].

$$SoH(t) = SoH(t-1) - \left[\eta_t(t-1) + \eta_{wz}(t-1)\right] \cdot \delta_t \tag{36}$$

where $\eta_T(t)[1/\text{sec}]$ is the coefficient associated with the battery temperature $(T(t))$ and $\eta_{wz}(t)[1/\text{sec}]$ is the working zone coefficient.

$$\begin{aligned} \eta_t(t) &= \alpha_t \left|T(t) - T_{ref}\right| + \beta_t \\ T(t) &= f\left(T_{env}(t), T(t-1), E(t)\right) \end{aligned} \tag{37}$$

f corresponds to a nonlinear function and T_{ref} to the reference temperature of the model (usually 10 °C). T_{env} (environmental temperature) can be estimated using the models presented in Section IV-E2,

$$\eta_{wz}(t) = \begin{cases} \eta_1 & \text{saturation or depletion} \\ \eta_2 & \text{overload or overdischarge} \\ \eta_3 & \text{load or discharge} \end{cases} \tag{38}$$

where $\alpha_T, \beta_T, \eta_1, \eta_2, \eta_3$ are experimental parameters. The saturation, overload, and load zones are defined based on the voltage; and the discharge, over-discharge and depletion zones are based on the energy of the ESS. It is important to note that η_1 is ten times greater than η_2 and η_2 is nearly two times greater than η_3

G. Water Supply Management

For the management of the water supply system, the tank system volume $V_T(t)$ is modeled as:

$$V_t(t) = V_t(t-1) + \delta_t w_f(t) - \delta_t w_c(t) \tag{39}$$

where $w_c(t)$ represents the water consumption. The water inflow into the tank $w_f(t)$ is given by:

$$w_f(t) = \kappa_t \eta_P P_P(t) = \kappa_t \eta_P \overline{P_P} B_P(t) \tag{40}$$

where k_T is a constant coefficient, η_P is the pump efficiency, and $P_P(t)$ is the pump power.

Adding a fictitious volume $V_{Tf}(t)$ to the tank model, the unserved water consumption is incorporated into the balance. Therefore, the volume of the tank is modeled by:

$$V_t(t) = V_t(t-1) + \delta_t \kappa_t \eta_P \overline{P_P} B_P(t) - \delta_t w_c(t) + V_{Tf}(t) \tag{41}$$

$$V_{Tmin} \leq V_t(t) \leq V_{Tmax}, V(T) \geq V_f, V_{Tf}(t) \geq 0 \tag{42}$$

where V_f is a reference value of the tank level.

For the optimizer, the water consumption can be predicted using historical data of the village.

H. Demand-Side Management

From [1], [27], it was supposed that online signals are sent to the consumers in order to modify their consumption behaviors, leaving daily energy constant. This modification is modeled by shifting coefficients $S_L(t)$ that are provided by the EMS. Therefore, the electric load is given by:

$$P_L(t) = S_L(t) \tilde{P}_L(t) \tag{43}$$

where $\tilde{P}_L(t)$ is the expected load. To take into account the maximum expected consumer response to the signals (empirical value), the shifting factor is bounded as:

$$S_{Lmin}(t) \leq S_L(t) \leq S_{Lmax}(t) \tag{44}$$

Additionally, it is assumed that the expected energy consumption could be bigger than the expected demand for the whole optimization period. This constraint is given by:

$$\sum_{t=T_1}^{T_2} P_L(t) \geq \sum_{t=T_1}^{T_2} \tilde{P}_L(t) \tag{45}$$

In addition to using T_1 to T_2 in (45), different sub periods for the energy balance can be defined for the optimization horizon (for example, energy balance for each day).

V. Case Study

The following results were obtained for a forecast horizon of 48 hours and a sampling time of 15 minutes. Note that the use of a 15 minute sampling time is reasonable for the proposed rolling horizon strategy as it is focused on energy management. As mentioned in Section IV-A, inside the 15 minute window, an ELD is used for the set points adjustments of the dispatchable generation units and the ESS. Additionally, the primary control of frequency and voltage are based on local control strategies implemented in each unit to face the faster variations of the renewable resources. Moreover, for the case study; Huatacondo village, at the north of Chile, there are important changes on the wind speed however the solar resource is more important, in terms of energy production, and has a lower variability inside the 15 minutes period.

The stochastic inputs for the optimizer are predicted for 192 steps ahead. For the evaluation purpose, the refresh rate of the sliding window (Δ) was 1 hour, or 4 periods. For the first case (PV/Diesel/ESS), the wind energy was not considered because the current system implemented in Huatacondo is operating with PV panels, a diesel generator and an ESS. In the second case, we analyze the advantages of incorporating the wind energy system into the microgrid (PV/Diesel/ESS/Wind). For this study, we considered two 2.5 kW wind turbines.

The irradiance for Huatacondo was obtained using the models described in Section IV-E, with the photovoltaic plant model considered as $\alpha = 0$. The wind speed was built using the measured data from Huatacondo and the models described in Section IV-E. Load consumption was forecast based on neural networks by considering the historical patterns of the location (see Section IV-E). All forecasts are updated every 15 minutes using the current data on the forecasting models as the EMS requires. A typical water consumption profile was considered, because there are not enough available measurement data for the training of a forecasting model.

Table I presents the prediction errors at 1 hour, 24 hours, and 48 hours ahead for the wind power, solar power and electric load, considering the following performance indexes: mean absolute percentage error (MAPE) and the root mean square error (RMSE). We observe that the prediction errors increase for longer horizon prediction.

A 48-hour forecast horizon was used because the battery state of charge at the end of the first day depends on both the weather conditions and the system electrical demand of the second day. The MIP optimization problem was solved using the commercial package CPLEX version 12.1 [28]

TABLE I
Prediction Errors

	1-hour ahead	24-hour ahead	48-hour ahead
Wind power			
MAPE [%]	11.73	24.67	27.50
RMSE [kW] (std)	0.42 (0.25)	1.24 (1.08)	1.48 (1.24)
Solar power			
MAPE [%]	8.14	11.19	11.35
RMSE [kW] (std)	1.26 (0.55)	1.37 (1.27)	1.43 (1.35)
Electric load			
MAPE [%]	9.27	12.59	14.59
RMSE [kW] (std)	1.36 (0.79)	2.25 (1.38)	2.68 (1.683)

As was mentioned in Section IV-A, a UC-RH is proposed for reducing the effect of the uncertainties of the input variable forecasting. To validate the proposed EMS-based UC-RH, a one-day-ahead UC was also implemented.

For evaluating both solutions (UC and UC-RH), the followings steps were achieved:

1) The EMS optimizes the system operation using the forecast data. For practical reasons (simplicity and accuracy), the optimization approach presented in Section IV-A was applied without the consideration of $C_H(T)$ and the related constraints.
2) The system operation is simulated using the set points obtained in step 1 and real data profiles (validation set). In this case, the output power of the units is adjusted to those defined by each data profile. For this task, a simplified version of an ELD model is used due the fact that only one unit (ESS or Diesel generator) is dispatchable in one specific period.
3) The costs are evaluated from the system operation simulated with the real data profiles.
4) The $C_H(T)$ cost is estimated for the different scenarios and added to the simulation costs for a complete analysis.

To evaluate the EMS performance, the following expected costs must be considered: the cost of operating the diesel generator (startup cost and operation cost), the unserved energy cost, and the opportunity cost of the energy stored in the LABB (energy deficit cost). Note that the opportunity cost, expressed as an energy deficit, is related to the difference between the reference energy value (E_f) and the energy value at the end of the period $(E(T))$. This value will be associated with the expected savings of using the diesel generator for providing the same amount of energy.

Consequently, the resulting EMS performance index is defined as follows:

$$\begin{aligned} Total\ expected\ cost &= Total\ Diesel\ cost \\ &+ Unserved\ Energy\ cost + Energy\ deficit\ cost \end{aligned} \tag{46}$$

A. EMS Results for a Microgrid (PV/Diesel/ESS)

In this case, the load-shifting capability is not considered $(S_{Lmin} = S_{Lmax} = 1)$. Figs. 6, 7 and 8 show the average value

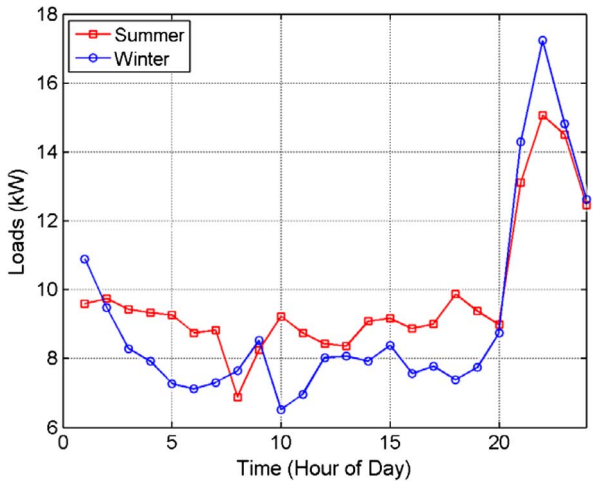

Fig. 6. Average load for the summer and winter seasons.

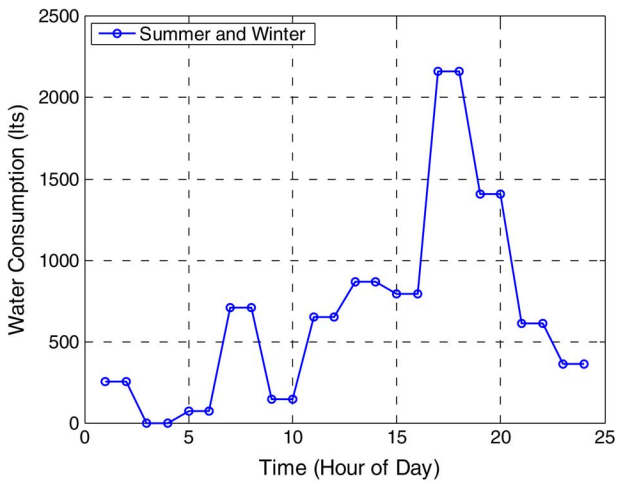

Fig. 7. Average water consumption for the summer and winter seasons.

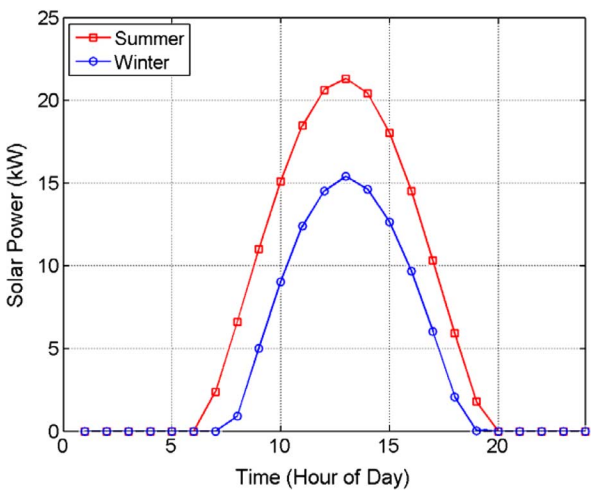

Fig. 8. Average solar power for the summer and winter seasons.

of the 500 samples for load, water consumption, and solar generation for both the summer and winter seasons. It can be observed a similar profile for the village load. Note that the same water consumption profile for both seasons is considered. In Fig. 8, different patterns for the irradiance according to the season are used.

TABLE II
SUMMER SEASON (PV/DIESEL/ESS)

		Control Strategy	
		UC	UC-RH
Cost [CLP$] (std)	Start-up, Diesel	2006	1173
	Operational, Diesel	19997	18192
	Total Diesel	22063 (1641)	18309 (1036)
	Energy Deficit	-1613	-1559
	Unserved Energy	0	0
	Total Costs EMS Performance	20450 (1855)	16750 (861)

TABLE III
WINTER SEASON (PV/DIESEL/ESS)

		Control Strategy	
		UC	UC-RH
Cost [CLP$] (std)	Start-up, Diesel	4891	1488
	Operational, Diesel	26836	24546
	Total Diesel	31727 (3465)	26034 (1581)
	Energy Deficit	2355	-1018
	Unserved Energy	1500	240
	Total Costs EMS Performance	35582 (3592)	25256 (1671)

Tables II and III show that the UC-RH reduces the expected total cost (18% for summer and 27% for winter) because of the lower start-up and operation diesel costs.

For the lower solar radiation in winter (see Fig. 8), the ESS operates close to its minimum energy capacity. Thus, if there is a forecasting error, it would be possible to reach values below the minimum. Consequently, the diesel generator starts up off schedule. Because the input forecasts considered by the UC-RH are updated at each step, this problem is reduced, and a lower start-up diesel cost is observed in comparison to the UC. For the summer season, the energy value is similar for both methods. In contrast, for the winter season, the UC generates positive energy values, meaning that the stored level of ESS energy is greater than the reference value E_f. When using the UC-RH, a greater value than the E_f energy level is achieved, and therefore, a significant energy saving is obtained. This phenomenon happens because the UC-RH looks further into the future than the UC, saving more energy for the limited energy of future winter conditions.

B. EMS Results for a Microgrid (PV/Diesel/ESS/Wind)

The energy supply system previously described can be improved by considering the advantage of wind energy integration. Using measured data from Huatacondo and the estimated error obtained from models described in Section V-E, 500 wind power profiles were built. Fig. 9 shows the average value of the 500 samples for wind power in summer and winter. In addition, RMSE resulting from the comparison between hourly wind forecasts and hourly measurements increase with the forecast range as shown in Table I.

Tables IV and V show a lower expected total cost (EMS performance index) than the PV/Diesel/ESS case (Section V-A) because of the wind energy contribution. Again, a total cost (EMS performance index) reduction is obtained using the UC-RH compared with the UC approach, which was observed for both seasons. However, the achieved savings (5% and 6%) are smaller than those in the previous case. The following additional interesting results should be noted:

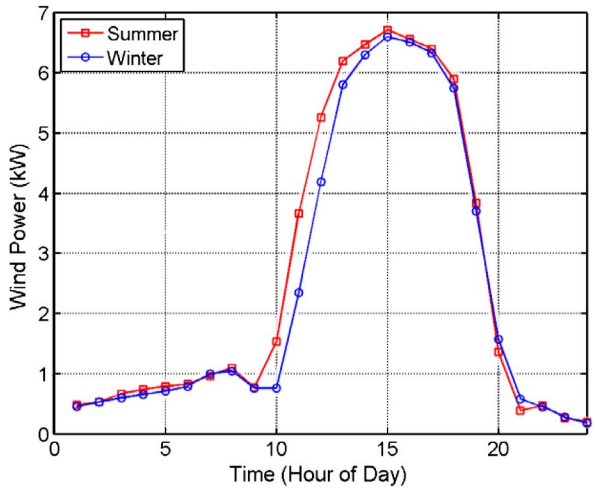

Fig. 9. Average wind power for summer and winter seasons.

TABLE IV
SUMMER SEASON (PV/DIESEL/ESS/WIND)

		Control Strategy	
		UC	UC-RH
Cost [CLP$] (std)	Start-up, Diesel	1850	1488
	Operational, Diesel	8419	9380
	Total Diesel	10269 (1589)	10868 (1299)
	Energy Deficit	2722	1472
	Unserved Energy	40	40
	Total Costs EMS Performance	13031 (1683)	12380 (1423)

TABLE V
WINTER SEASON (PV/DIESEL/ESS/WIND)

		Control Strategy	
		UC	UC-RH
Cost [CLP$] (std)	Start-up, Diesel	1719	1718
	Operational, Diesel	12687	13896
	Total Diesel	14406 (3168)	15614 (2740)
	Energy Deficit	3210	930
	Unserved Energy	300	140
	Total Costs EMS Performance	17916 (2406)	16683 (1912)

- The expected operational diesel costs are higher in the case of UC-RH. This can be explained by seeing the corresponding energy deficit costs that also impose "future operational costs" for the system. In fact, taking into account the sum of these two costs, it can be concluded that the UC-RH approach shows lower operational costs (operational diesel plus energy deficit costs) for the period. For example, from Table IV, these operational costs are $\mathrm{CLP\$11141(CLP\$8419 + CLP\$2722)}$ for the UC approach and $\mathrm{CLP\$10852(CLP\$9380 + CLP\$1472)}$ using the UC-RH.
- During the summer, there is unserved energy, which was not present in the previous case. The reason for this could be the uncertainties associated to the forecasted wind speed.
- The UC-RH reduces the energy deficit. This phenomenon grows in the winter because there is less available energy (Figs. 8 and 9) and the diesel generator is used intensively.

TABLE VI
LABB INVESTMENT COSTS

	UC PV/DIESEL ESS	UC-RH PV/DIESEL ESS	UC PV/DIESEL ESS/WIND	UC-RH PV/DIESEL ESS/WIND
Initial investment [MM CLP$]	10.0	10.0	10.0	10.0
Life cycles over 20 years [#]	12445	11432	10585	10552
Lifetime [years]	1.37	1.49	1.61	1.61
Investment cost over 20 years (replacement costs) [MM CLP$]	60.3	55.3	50.8	50.7
LABB Total costs [MM CLP$]	70.3	65.3	60.8	60.7

TABLE VII
DIFFERENCE IN INVESTMENT AND OPERATIONAL COSTS FOR THE ALTERNATIVE CONFIGURATIONS

	UC PV/DIESEL ESS	UC-RH PV/DIESEL ESS	UC PV/DIESEL ESS/WIND	UC-RH PV/DIESEL ESS/WIND
LABB Total costs [MM CLP$]	70.3	65.3	60.8	60.7
Wind-turbine investment [MM CLP$]	0	0	5.6	5.6
Diesel operational costs [MM CLP$]	84.7	64.9	47.6	44.9
Total costs [MM CLP$]	155.0	130.2	114.0	111.2
Cost difference [MM CLP$]	24.8		2.8	

C. Overall Analysis

For evaluating the overall performance of the two microgrid configurations, the investment and operational costs of the main units are analyzed over a period of 20 years (This period corresponds to the wind turbine lifetime). Specifically, the investment is calculated for the LABB and the wind turbine units.

The operational costs presented here are obtained from the results shown in Sections V-A and V-B. We assume a constant demand pattern over the evaluation period.

The LABB costs are detailed in Table VI. It includes the initial investment costs of the battery bank (first row) and the replacement costs based on the life cycles over 20 years obtained from the EMS operation results (ex-post evaluation).

Finally, the total cost of the LABB is summarized for the two optimization approaches (UC and UC-RH). 850 rated life cycles at 80% discharge depth are considered in the evaluation based on the manufacturer data. The net present value is calculated with a discount rate of 10%, which is a common value used in the Chilean energy sector.

The difference in investment and operational costs for the two microgrid configurations are summarized in Table VII. This table shows a lower total cost for the PV/Diesel/ESS/WIND solution for both the UC and UC-RH approaches. Additionally, for both configurations, a cost reduction using UC-RH over UC is observed.

TABLE VIII
SUMMER SEASON (PV/DIESEL/ESS) EMS/DSM/UC-RH

		S_{Lmin} / S_{Lmax}			
		1.0/1.0	0.95/1.05	0.9/1.1	0.85/1.15
Cost [CLP$]	Start-up, Diesel	1000	1000	1000	1000
	Operational, Diesel	14424	12264	11487	10564
	Total Diesel	15424	13264	12487	11564
	Unserved Energy	0	0	0	0
	Total Costs	15424	13264	12487	11564

From the overall results, we observe that the total costs (investment and operational) of PV/Diesel/ESS/Wind are up to 15% lower than the PV/Diesel/ESS for the case of rolling horizon (RH). Actually, for this case, the additional investment costs of the wind turbine are less than the reduction in the operational costs.

D. EMS Results With a DSM

To show the advantages of the DSM, Table VIII presents the results of the proposed EMS using the UC-RH for the microgrid (PV/Diesel/ESS). In this table, different shifting factor bounds of the electric demand (S_{Lmax}, S_{Lmin}) are applied using a typical demand and an irradiance profile for the summer season. Additionally, it is important to note that the performance evaluation is based on the optimizer results.

The total cost decreases as the demand shifting coefficients are made more flexible. This result is expected, given that EMS was designed for generating signals to consumers. Thus, the system load is shifted to periods when the solar energy is available. In addition, the diesel operation is optimized, increasing its efficiency. The former improves fuel management usage.

VI. CONCLUSIONS

This paper presents a novel energy management system for a renewable-based microgrid. The EMS provides the online set points for generation units while minimizing the operational cost and considering the forecast of renewable resources, load and water consumption.

The results of the EMS showed the economic benefit of the proposed unit commitment with a rolling horizon (UC-RH) in comparison with a standard UC. The rolling horizon presents the advantage of dealing with updated data from the forecast variables. The average operational costs of the microgrid (PV/Diesel/ESS) using the UC-RH are reduced for certain profiles of demand and irradiance in comparison with the UC. For the case of the wind-based microgrid (PV/Diesel/ESS/Wind), the operational costs are also reduced because of a reduction in the energy deficit, implying a better management of the ESS in comparison with the UC approach. The previous results are verified for two alternative microgrid configurations. In fact, the overall analysis, that include both operational and investment costs, re-confirms that for both microgrid configurations, the UC-RH solution provides lower total costs than a standard UC approach.

Additionally, note that both UC and UC-RH strategies require the same communication infrastructure, just a faster updated of unit set-points is required with UC-RH.

The benefits of DSM are also shown in this paper. Those benefits are achieved by means of shifting the behavior of consumers to periods in which there are more renewable resources available.

TABLE IX
PARAMETERS (1 US Dollar = 500 CLP$.)

Name	Variable	Value	Unit
Min Diesel Power	P_1^{min}	10	kW
Max Diesel Power	P_3^{max}	120	kW
Max ESS Power	P_{Bmax}	40	kW
Max LABB Capacity (C_{10})	E_{max}	117	kWh
Rated PV Power	-	22	kW
Rated Wind Power	-	5	kW
Max Load Power	-	28	kW
Min Load Power	-	3.2	kW
Max Water Consumption	w_{Cmax}	2500	l/h
Rated Pump Power	$\bar{P}_P$	1	kW
Unserved Energy Cost	C_{US}	250	CLP$/kWh
Unserved Water Cost	C_{Tf}	520	CLP$/l
Diesel Start-up Cost	C_S	1000	CLP$
Diesel Price	C_C	500	CLP$/l
Reference Energy Value	E_f	90	kWh

The proposed EMS allows efficient management of the water supply by optimizing the water pump activation as a flexible load, especially for periods with energy surplus. The EMS for a microgrid displays the attributes of a smart grid by providing optimized set points for electrical units. Moreover, it also considers other services by integrating water and electric load demands.

In the next step of this work, the proposed EMS will be implemented at the specific location in the Atacama Desert. The effect of prediction errors and a sliding window optimization will be included. Field measurements, the behavior of the communication platform, the dynamic response of the system and adjustments of the proposed EMS will be reported. From the results, the integration of computational intelligence techniques in forecasting and control strategies is envisioned. Future research will also focus on the incorporation of the proposed LABB penalty cost model in the optimization procedure.

APPENDIX

Further detailed technical characteristics of the microgrid units are summarized in Table IX.

REFERENCES

[1] R. Palma-Behnke, C. Benavides, E. Aranda, J. Llanos, and D. Sáez, "Energy management system for a renewable based nicrogrid with a demand side management mechanism," in *Proc. 2011 IEEE Symp. Comput. Intell. Appl. Smart Grid (SSCI 2011 CIASG)*, Paris, France, Apr. 11–15, 2011.

[2] Office of Electricity Delivery and Energy Reliability, U.S. Department of Energy, "The smart grid: An introduction," 2010 [Online]. Available: http://www.oe.energy.gov/1165.htm

[3] A. Hajizadeh and M. Aliakbar Golkar, "Intelligent power management strategy of hybrid distributed generation system," *Electr. Power Energy Syst.*, vol. 29, pp. 783–795, 2007.

[4] P. Lombardi, M. Powalko, and K. Rudion, "Optimal operation of a virtual power plant," in *Proc. IEEE Power Energy Soc. Gen. Meet. (PES)*, 2009.

[5] D. Lu and B. Francois, "Strategic framework of an energy management of a microgrid with a photovoltaic-based active generator," in *Proc. EPE Chapter "Electric Drives" Joint Symp. (ELECTROMOTION 2009)*, Lille, France, Jul. 1–3, 2009.

[6] S. Teleke, M. Baran, S. Bhattacharya, and A. Huang, "Rule-base control of battery energy storage for dispatching intermittent renewable sources," *IEEE Trans. Sustainable Energy*, vol. 1, no. 3, pp. 117–124, 2010.

[7] C. Wang and M. Hashem, "Power management of a stand-Alone wind/photovoltaic/fuel cell energy system," *IEEE Trans. Energy Convers.*, vol. 23, no. 3, pp. 957–967, 2007.

[8] A. Gupta, R. Saini, and M. Sharma, "Steady-state modelling of hybrid energy system," in *Proc. 3rd Int. Conf. Electr. Eng. (ICEE)*, 2009.
[9] D. Westermann and A. John, "Demand matching wind power generation with wide-area measurement and demand-side management," *IEEE Trans. Energy Convers.*, vol. 22, no. 1, pp. 145–149, 2007.
[10] V. Hamidi and F. Robinson, "Responsive demand in networks with high penetration of wind power," in *Proc. IEEE Power Energy Soc. Gen. Meet.—Convers. Del. Electr. Energy 21st Century*, 2008.
[11] J. Lagorse and M. Somoes, "A multiagent fuzzy-logic-based energy management of hybrid systems," in *Proc. IEEE Ind. Appl. Soc. Annu. Meet. (IAS)*, 2009.
[12] T. Logenthiran and D. Srinivasan, "Short term generation scheduling of a microgrid," in *Proc. IEEE Region 10 Conf. (TENCON 2009)*.
[13] A. Tsikalakis and N. Haatziargyriou, "Centralized control for optimizing microgrids operation," *IEEE Trans. Energy Convers.*, vol. 23, no. 1, pp. 241–248, 2008.
[14] H. Dagdougui, R. Minciardi, A. Ouammi, M. Robba, and R. Sacile, "A dynamic decision model for the real-time control of hybrid renewable energy production systems," *IEEE Syst. J.*, vol. 4, no. 3, pp. 323–333, Sep. 2010.
[15] H. Morais, P. Kádár, P. Faria, Z. Vale, and H. Khodr, "Optimal scheduling of a renewable micro-grid in an isolated load area using mixed-integer linear programming," *Renewable Energy*, vol. 35, no. 1, pp. 151–156, Jan. 2010.
[16] M. Korpas and A. Holen, "Operation planning of hydrogen storage connected to wind power operating in a power market," *IEEE Trans. Energy Convers.*, vol. 21, no. 3, pp. 742–749, 2006.
[17] Matrikon OPC [Online]. Available: http://www.matrikonopc.com/
[18] R. Teodorescu, M. Liserre, and P. Rodríguez, *Grid Converters for Photovoltaic and Wind Power Systems*. New York: Wiley-IEEE, 2011.
[19] H. Beyer, J. Martínez, M. Suri, J. Torres, E. Lorenz, S. Müller, C. Hoyer-Klick, and P. Ineichen, "Report on benchmarking of radiation products," Sixth Framework Programme MESOR, Management and Exploitation of Solar Resource Knowledge, 2009 [Online]. Available: http://www.mesor.org/docs/MESoR_Benchmarking_of_radiation_products.pdf
[20] V. Zavala, E. Constantinescu, and M. Anitescu, "Economic impacts of advanced weather forecasting on energy system operations," in *Proc. Innov. Smart Grid Technol. (ISGT)*, 2010.
[21] W. Skamarock, J. Klemo, J. Dudhia, D. Gill, D. Barker, M. Duda, X. Huang, W. Wang, and J. Powera, "A description of the Advanced Research WRF Version 3," Tech Rep. 475+STR, NCAR, 2008.
[22] Z. Bashir and M. El-Hawary, "Applying wavelets to short-term load forecasting using PSO-based neural networks," *IEEE Trans. Power Syst.*, vol. 24, no. 1, pp. 20–27, 2009.
[23] V. Hinojosa and A. Hoese, "Short-term forecasting using fuzzy inductive reasoning an evolutionary algorithms," *IEEE Trans. Power Syst.*, vol. 25, no. 1, pp. 565–574, 2010.
[24] M. Norgaard, O. Ravn, N. Poulsen, and L. Hansen, *Neural Networks for Modelling and Control of Dynamic Systems*. New York: Springer-Verlag, 2000.
[25] H. Bergveld, *Battery Management Systems Design by Modelling*. Eindhoven, The Netherlands: Univ. Press Facilities, 2001.
[26] D. Guasch and S. Silvestre, "Dynamic battery model for photovoltaic applications," *Progr. Photovoltaics: Res. Appl.*, vol. 11, pp. 193–206, 2003.
[27] R. Palma-Behnke, D. Ortiz, L. Reyes, G. Jiménez-Estévez, N. Garrido, and N. , "A social SCADA approach for a renewable based microgrid," in *The Huatacondo Project, 2011 IEEE Power Energy Soc. Gen. Meet.*, Detroit, MI, Jul. 24–28, 2011.
[28] CPLEX [Online]. Available: http://www-01.ibm.com/software/integration/optimization/cplex-optimizer/

Rodrigo Palma-Behnke (S'03) received his B.Sc. and M.Sc. degrees in electrical engineering from the Pontificia Universidad Católica de Chile and a Dr.-Ing. from the University of Dortmund, Germany.

He is currently an Associate Professor in the Electrical Engineering Department at the University of Chile. His research field is the planning and operation of electrical systems in competitive power markets and new technologies.

Carlos Benavides received his B.Sc. and M.Sc. degrees in electrical engineering from the University of Chile. His research field is the planning and operation of electrical systems in power markets.

Fernando Lanas received his B.Sc. degree in electrical engineering from the University of Chile in 2011. His main research interest is the planning and operation of hybrid energy systems based on renewable resources.

Bernardo Severino received his B.Sc. degree in electrical engineering from the University of Chile in 2011. His main research interest is modeling energy storage systems for microgrids.

Lorenzo Reyes received his B.Sc. degree in electrical engineering from the University of Chile in 2009. His main research interest is microgrid development.

Jacqueline Llanos (M'11) received her electronic engineering degree from the Escuela Politécnica del Ejercito, Ecuador, and her M.Sc. in electrical engineering from the University of Chile. Her research fields are predictive control, forecasting of electricity demand, and renewable resources.

Doris Sáez (SM'05) received her M.Sc. and Ph.D. degrees in electrical engineering from the Pontificia Universidad Católica de Chile.

She is currently an Associate Professor in the Electrical Engineering Department at the University of Chile. Her research fields are fuzzy systems control design, fuzzy identification, predictive control, control of power generation plants, and control of transport systems.